# DocuServe

## Electronic Delivery Cover Sheet



## Caltech Library Services

Acta Astronautica 170 (2020) 443–451

Contents lists available at ScienceDirect

Acta Astronautica

journal homepage: www.elsevier.com/locate/actaastro

Research paper

# An ultralight concentrator photovoltaic system for space solar power harvesting

Emily C. Warmann[a,*], Pilar Espinet-Gonzalez[a], Nina Vaidya[a], Samuel Loke[a], Ali Naqavi[a], Tatiana Vinogradova[b], Michael Kelzenberg[a], Christophe Leclerc[c], Eleftherios Gdoutos[c], Sergio Pellegrino[c], Harry A. Atwater[a,d]

[a] Thomas J. Watson Laboratories of Applied Physics, California Institute of Technology, Pasadena, CA, 91125, USA
[b] Northrop Grumman Aerospace Systems, 1111 W 3rd St, Azusa, CA, 91702, USA
[c] Graduate Aerospace Laboratories, California Institute of Technology, Pasadena, CA, 91125, USA
[d] Kavli Nanoscience Institute, California Institute of Technology, Pasadena, CA, 91125, USA

A B S T R A C T

We present a detailed design treatment for a concentrating photovoltaic mini module subsystem with a specific power of up to 4.1 kW/kg for integration into a space solar power system. Concentrating designs are required to achieve specific power over 1 kW/kg with current high-efficiency III-V multijunction solar cells. The 15 sun, linear concentration concept detailed here reduces the system mass by replacing cell and radiation shield area with ultralight carbon fiber reinforced polymer (CFRP) optics. Reducing the cell size to 1 mm width as well as careful optimization of cell architecture and CFRP material and thickness are critical for maintaining cell temperatures under 100 C despite the concentration. We also describe ultralight multilayer optical coatings to increase the thermal emissivity of the concentrator surfaces and enhance radiative transfer for cell cooling, which is a critical technological component of the total system design.

## 1. An ultralight concentrator photovoltaic system for space solar power harvesting

THE vision of generating power in space and beaming it to earth to replace terrestrial electricity generation has tantalized futurists since Asimov imagined it in 1947 [1]. Technical evaluation of this concept began almost as soon as solar photovoltaics (PV) became established as a viable generation technology for space, yet every iteration of this analysis has concluded that the cost of such a system would make the energy generated too expensive to compete with terrestrial sources [2–5]. The high cost of a space-based solar power (SSP) system is not solely determined by the costs of the solar cells and transmission electronics themselves, as the cost of launching the mass required can be the largest component of the total cost. Consequently the technology has been perceived as infeasible without a dramatic reduction in launch costs, with such a reduction remaining far beyond the technology horizon.

Recent improvements in the efficiency of solar cells and power electronics have again sparked renewed interest in the SSP concept. New system designs have been proposed, making use of lightweight deployable spacecraft and phased-array antennas [6,7], The Japanese and Chinese space agencies are both pursuing research in microwave power beaming for transfer of power from orbit in a space solar power application [8–10] and the US Office of Naval Research is pursuing testing of an integrated device combining photovoltaics and power beaming components in a compact package with the vision of scaling to larger area in the future [11]. To date, SSP design efforts use conventional space photovoltaics cells similar to those used on commercial satellites and solar-powered space probes, which are highly efficient yet costly compared to terrestrial solar panels. While space PV manufacturers have development efforts underway to increase efficiency and reduce the weight of cells, these are incremental improvements that will provide only a marginal increase in specific power and will result in a space solar power system with, again, prohibitive launch costs in the absence of a transformative new launch technology [3].

An alternate approach, which we have detailed previously [12,13], is to make a radical reduction in the mass of the solar power system, combined with an efficient packaging and deployment scheme, such that the number of launches required to deploy the system decreases to the point that the total launch costs are acceptable even at current launch capabilities. Reducing the system mass to this extent requires designing a new photovoltaic array for space with a power to mass ratio (specific power) of 1–10 kW/kg. This specific power range is one to two orders of magnitude higher than that of current space photovoltaic

* Corresponding author.
*E-mail address:* warmann@caltech.edu (E.C. Warmann).

https://doi.org/10.1016/j.actaastro.2019.12.032
Received 25 June 2019; Received in revised form 18 December 2019; Accepted 24 December 2019
Available online 27 January 2020
0094-5765/ 

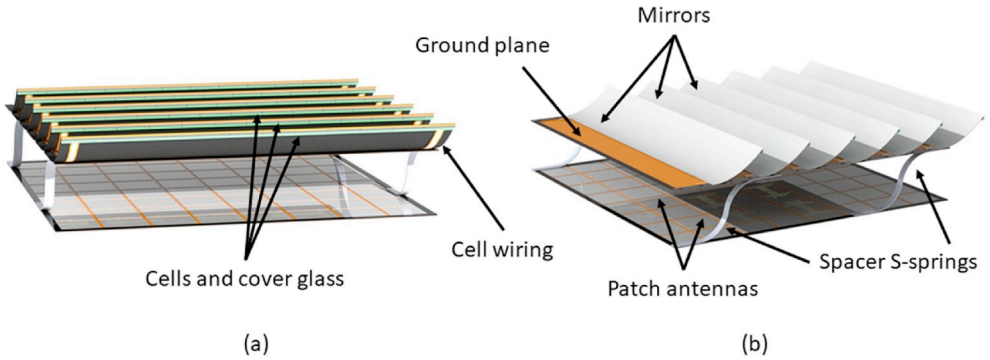


**Fig. 1.** Conceptual visualization of the space solar power tile. The linear concentrating mirrors are mounted on the top of the ground plane with the cells on the back sides of the mirrors, shown in a rear view in panel (a). The power conversion electronics are located under the ground plane and the antenna plane is separated from the ground plane at ¼ wavelength distance by the S-springs.

array designs [14,15], and can be considered an equivalent reduction in the launch cost per kW, bringing the concept of space based solar power closer to economic feasibility. If such a system can be made at low cost per watt, similar to terrestrial photovoltaics and at the gigawatt scale, the high capacity factor of PV at geostationary orbit will make the power generated competitive with current baseload generation systems.

In previous work we have described a full system point design including the photovoltaics, microwave transmission electronics and antenna array, and the modular structural and deployment concept [13]. This design is based on a modular unit combining photovoltaics, power conversion electronics and antennas for all-local power conversion to eliminate the need for a large-scale power bus. The base unit of the design is a tile, shown in Fig. 1 as a conceptual image. Here we explore the design space and present a detailed technical design of the photovoltaics subsystem capable of meeting overall system requirements for integration with the structural and transmission electronics subsystems. For the PV subsystem, this design is capable of specific power of up to 4.1 kW/kg, meeting the PV efficiency requirements of the system concept at an overall (PV + power conversion electronics + antenna) specific power of 0.5–1 kW/kg, though prototyping efforts have not yet reached that performance level. This design is the foundation of our current prototyping efforts aimed at validating the optical and electronic design as well as the local integration with microwave transmission in a self-contained, modular “tile” unit.

## 2. Design approach – low, single-axis concentration

A photovoltaic array in space must serve multiple functions while minimizing total mass. The system must create an optical path for incident sunlight while shielding the cells from damaging high energy particle radiation. The array must provide a thermal pathway for waste heat to be conducted away from the cells and radiated to space to maintain an acceptable cell temperature. Finally the array must provide mechanical support to maintain the optical aperture through orbital manoeuvers. The system must perform all of these functions reliably, and within strict degradation limits, over the course of years or decades of service. In current high specific power flat plate designs, the bulk of the system mass comprises the radiation shielding, cell encapsulation and the photovoltaic cells [16]. The mass of the heat conduction and mechanical support components of the system are comparatively small. Our design approach, moderate concentration on a single axis, directly reduces these primary mass components while maintaining a low mass for the thermal and structural functions of the design.

Concentration to increase cell efficiency and reduce system cost is an established technology for terrestrial applications but development for space deployment has lagged. In the late 1990s, early versions of the Hughes/Boeing 702 spacecraft used large, fold-out reflector panels on either side of the solar wings, which increased the array power by ~1.8x, but which also increased the panel temperature from ~60 °C to ~120 °C. Unfortunately, the optical components suffered premature degradation as volatile compounds out-gassed from the cell encapsulation material, condensed on the reflecting surfaces, and subsequently darkened due to UV exposure [17]. Although this failure originated from encapsulant outgassing, non-concentrating solar panels of similar construction had operated flawlessly on other spacecraft. This illustrates two intrinsic challenges for photovoltaic concentrators in space: limiting the temperature rise, and protecting the concentrator optics from contamination, deformation, or other damage in the space environment. The 702 concentrators were quickly abandoned, and the commercial satellite community has conservatively focused on incremental improvements to current flat plate designs.

To prevent excessive rise in cell temperatures associated with concentration, it is necessary to use heat spreaders and radiators to increase the area over which waste heat can be radiated away. Several concentrator designs have been developed using this principle, including stretched lens arrays [18] and line- and point-focus lens arrays with graphene radiators [19,20]. The parabolic trough concentrator geometry (shown in Figs. 1 and 3) is particularly promising from a mass reduction standpoint, because each reflector can also serve as the heat spreader, radiator, and mechanical mount for the adjacent photovoltaic cell, while further providing moderate radiation shielding. In principle, very little material is required to form a high-quality reflective concentrator; on the order of 50 nm of Ag or Al forms a highly reflective mirror. The remainder of the material required serves to provide adequate thermal conductivity, structural rigidity, durability, and thermal emissivity. By contrast, refractive concentrators generally require thicker focusing optics such as Fresnel lenses, several 10s of microns thick to achieve similar efficiencies, in addition to separate cell support and heat spreading components. Although some refractive designs offer improved tolerance to lens misalignment vs. reflective designs [18], our preliminary studies showed optical efficiency comparable or better for the parabolic trough compared to Fresnel lenses [20]. Together, these factors enable much higher specific power for this concentration design compared to other concepts in development. This geometry was pioneered for space by the SLATS and FAST programs [21,22]. Our design is based on this approach, optimized for the modular tile concept of Fig. 1, and incorporating recent advances in photovoltaics, photonics, and ultralight composites.

The mass reduction benefits of concentration stem from exchanging thick, massive cell radiation shielding material for lower-mass reflecting optics. The extent of the benefits for a particular design are determined by the amount of additional material required to conduct heat away from the cell and radiate it to space. To explore this trade-off for a linear trough concentrator, we simulated cell temperature as a function of concentration, mirror thermal conductance, surface emissivity and cell size using COMSOL. The steady state, 2D finite element method (FEM) simulation geometry assumed an array of five mirrors of infinite length, with an opaque ground plane at the base of the mirrors for mounting support and representing the other SSP system components. The power beaming components here have no internal heat generation and serve only to obscure emission from the back side of the cell and mirror array. Modeling an array rather than a single mirror

allows us to capture the effect of internal reflection and absorption of thermal radiation. While temperatures were monitored throughout the array, the temperature of the central cell, being highest due to receiving heat emitted from adjacent cells as well as having a reduced view of the cold background was chosen as the evaluation parameter for all design iterations. Increasing the array to seven mirrors resulted in negligible increase in the cell in the central position, indicating an array of five mirrors represents the best tradeoff of modeling accuracy and speed for these simulations. The cells are 10 μm thick III-V triple junctions (assumed 30% efficiency) on 20 μm copper back supports and protected from radiation by 100 μm of ceria-doped cover glass and the thickness of the CFRP (assumed isotropic, with thermal conductivity 90 W/m-K) mirror is sufficient to conduct heat from the cell to maintain a temperature of 100 C, assuming cells with a one-sun heat load of 650 W/m$^2$ (scaled by the concentration ratio for each iteration). The rear surface emissivity is assumed to be 0.88 and the mirror surface emissivity is 0.1. Material parameters were chosen based on the materials and design approaches described in subsequent sections of this paper. This first-order calculation is useful for determining the optimal concentration ratio and the upper limit for specific power, given our design assumptions and materials selections. However, the calculation does not include all sources of mass, such as cell wiring, panel frame, backing, or adhesives; thus, it should be understood that a complete concentrator subsytem will have lower specific power, as detailed in subsequent sections.

The results are shown in Fig. 2. In panel (a), the plot shows the mass components for a design with 1 mm wide cells. As the plot shows, the mass required for radiation shielding and cells drops rapidly with concentration, because the area fraction occupied by the cells and shields is inversely proportional to the concentration ratio. Conversely the mass required to conduct heat away from the cells increases with the concentration, because the amount of waste heat dissipated in the cells is directly proportional to the concentration. Assuming that the mass required for structural support is independent of the concentration, these two trends combine to result in a maximum for the power per mass or specific power at around 15 suns for 1 mm wide cells. For comparison, a flat plate design with the same cells, cover glass and mechanical support would have an area mass density of ~450 g/m$^2$ and specific power of ~1 kW/kg, thus the concentration approach can increase the specific power by a factor of ~12.

Fig. 2, panel (b) shows the specific power vs concentration for cells ranging from 1 to 50 mm in width, again with 100 μm cover glass and carbon fiber thickness selected to maintain cell temperature at 100C. As panel (b) shows, the optimum concentration and specific power are determined by the width of the solar cell in the linear concentrator. Assuming all other optical components of the system have constant mass, the difference is driven by the increasing amounts of material needed to conduct heat away from the cell to maintain the operating temperature at 100 C, an upper bound temperature of operation that will allow long life for conventional cells [23]. While the trade-off between concentration and mass for thermal conduction shown in Fig. 2 (b) implies further gains from cell miniaturization below 1 mm and subsequent increased concentration, this benefit must be weighed against the reduction in acceptance angle for higher concentration designs, difficulties in fabricating and aligning such small concentrators, and increasing parts count. Our design approach has identified reducing cell width to 1 mm as a key parameter for achieving high specific power at acceptable cell temperatures while maintaining reasonable acceptance angle. In the following sections we will detail additional key technical achievements that are essential to achieving ultra-high specific power in a concentrating space PV system.

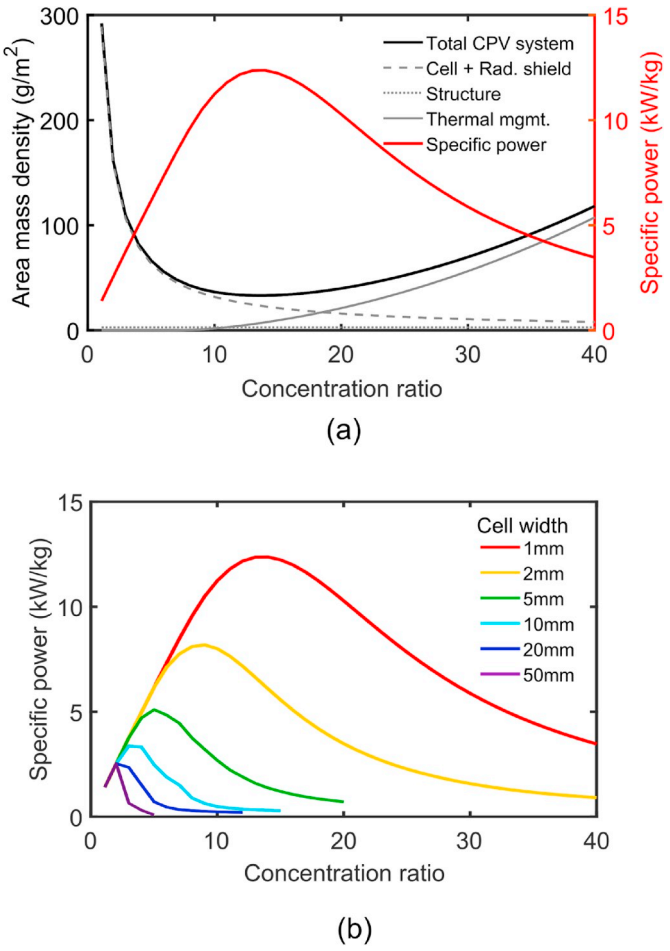


**Fig. 2.** Panel (a), plot of the area mass density and specific power vs concentration for a CPV system with 1 mm wide cells covered by 100 μm thick cover glass. The thermal management material is sized to maintain a cell temperature of 100 C under concentration. In panel (b), specific power vs concentration for cells of width ranging from 1 to 50 mm.

### 2.1. Ultralight concentrating optics

The concentrating element of our design is a linear parabolic trough reflector that focuses light onto cells mounted on the upper portion of the back side of the adjacent reflector, as shown in schematic form in Fig. 3. The cell mounting position both reduces shadowing losses and allows the mirror to serve as a conductive pathway to remove heat from the cell. This concentration configuration is very similar to that of the SLATS experiment, however our design achieves higher specific power through cell miniaturization and maximizing the thermal conductivity of the optics. In addition, the design is intended to be folded flat and further packaged for launch and to self-deploy. This design achieves these multiple functions, thermal conductance, mass reduction and flexibility for packaging, through the use of ultralight carbon fiber reinforced polymer (CFRP) composite materials. Carbon fiber reinforced polymers are well suited for this application, and have been investigated for use in space telescope optics in addition to longstanding history of space structural applications [24,25]. Compared to prior concentrators of this style, such as the SLATS experiment, our design seeks to achieve higher specific power through cell miniaturization as discussed above, which means that extremely thin (< 100 μm) CFRP concentrator fins are adequately thermally conductive to cool the cells. At this thickness range, CFRP has the added benefit of being flexible and highly elastic. Thus, the concentrators can be folded flat for efficient packaging for launch and will self-deploy when unpacked due to the strain energy stored in the composite.

The lightweight parabolic reflector fabrication process begins by casting 3- or 4-ply CFRP sheets over a parabolic mold, using thin unidirectional prepreg material comprised of high thermal conductivity

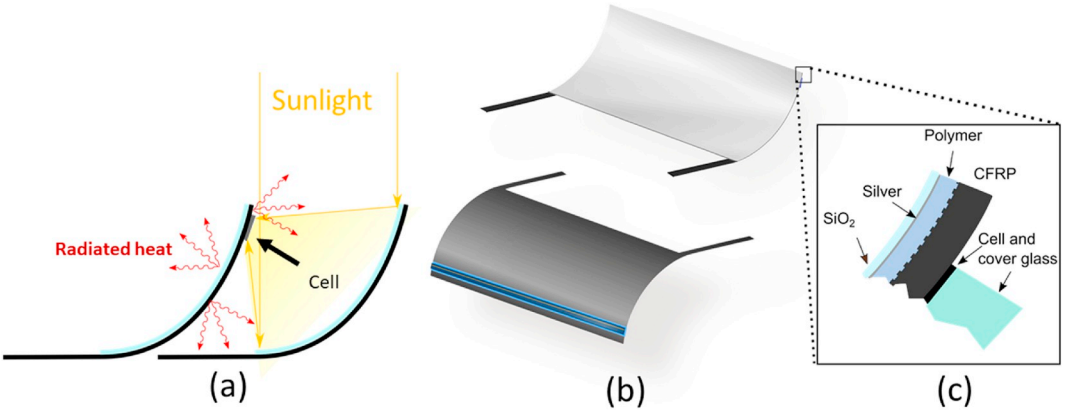


**Fig. 3.** Schematic representation of the linear concentration concept. Panel (a) shows a cross-sectional view. The cell is located on the back of the adjacent reflector, backset slightly from the edge, to prevent shadowing losses. Heat is conducted away from the cell via the CFRP reflector material and radiated to space. Panel (b) shows top and bottom views of the reflector structures. On the front, reflecting side, the CFRP is covered with a smoothing polymer, silver mirror and a highly emissive layer, shown in inset (c) (not to scale).

pitch fibers [26]. The lay-up configuration is symmetric, with the outer two layers having fibers oriented along the curvature of the parabola (90°) sandwiching one or two inner layers with fibers parallel to the concentrator axis (0°). The outer plies provide the composite with adequate thermal conductivity. The mold shape is tailored to produce reflectors with the correct final parabolic shape after the CFRP has been cured at elevated temperature, cooled, released, and trimmed to shape via laser cutting [27].

Fig. 3 panel (b) shows the finished shape of the mirrors from the top and bottom views with the reflective coating added and the cells mounted on the back side. The two features extending from the bottom edge of the mirror allow the reflector to be mounted to the other structural elements of the tile. The as-cast CRFP surface cannot be directly coated with metal to produce a specular reflector, because the surface texture is too rough. We have previously reported a smoothing process in which a thin UV-cured polymer coating is applied to the CFRP surface prior to evaporating Ag to produce a specular and highly reflective mirror surface [28,29]. In addition to smoothing the micro-scale roughness of the CFRP, the polymer coating must also be able to tolerate temperatures in excess of 100C to be compatible with the cells under concentration and the material must have minimal out-gassing to qualify for the space environment. Our design uses a UV curing, space-grade epoxy product, such as Masterbond UV22DV80-1 applied to the surface by draw-down process [30,31]. The epoxy surface of the reflector that faces the sun is coated with ~40 nm of Ag protected by 10–20 nm of $SiO_2$ for efficient optical reflection across the spectrum. Fig. 3 panel (c) shows a cross section of the mirror with the smoothing layer and reflective coatings (not to scale).

Based on a ray trace analysis of this concentrator design, a mirror with 15 suns concentration will have a geometrical optical efficiency of 98% averaged over a total 2.5° acceptance angle (1.25° half angle) around the axis of concentration. This acceptance is much broader than the solar solid angle and well within the pointing accuracy capabilities of modern space craft [32]. Because the acceptance angle and concentration ratio are geometrically linked, that acceptance angle could be doubled by halving the concentration to 7.5 suns, either by reducing the aperture or doubling the cell width.

The acceptance angle around the secondary axis is determined by the length of the troughs, as light escapes the open ends of the mirrors when tilted lengthwise. Current prototypes feature mirrors of 10 cm length, which retain 74% optical efficiency up to 45° of tilt, allowing the array to be maneuvered in one axis to facilitate power beaming. If mirror accuracy can be maintained at greater lengths or if troughs can be aligned precisely end to end, this loss can be reduced. Once coated with a high-quality protected silver mirror with 97.5% reflectivity over the AM0 spectrum, the 15x concentrator can achieve a total optical efficiency of 95.7% at normal incidence. Initial prototype efforts have produced individual mirrors with optical efficiency as high as 92% and whole-tile optical efficiency of 88%.

While the nominal design of the 15x concentrator offers a reasonable 2.5° ( ± 1.25°) any manufacturing process will result in some degree of variation in the shape and size of the mirrors and their alignment with respect to the adjacent cells, which could reduce the optical efficiency or acceptance angle of the ensemble concentrator assembly. To help quantify the degree of assembly precision required for these designs, we conducted Monte Carlo raytracing simulations of the concentrators accounting for several potential sources of manufacturing error. Specifically, we considered errors in the reflector-to-reflector spacing, errors in the cut length of each reflector, errors in the positioning of the cells on the rear of each reflector, and errors in the parabolic coefficient of the mirrors, as shown schematically in Fig. 4(a). The simulation picks random values for each error source at both ends of each concentrator element and assumes that the profile and position of the components varies linearly along the length of the reflectors. For each error source, we use a normal random distribution, and for simplicity, we use the same value of standard deviation for all error sources, with the following two exceptions: (1), for the parabolic coefficient, we assign a standard deviation value that yields a distribution of mirror-end deflections with approximately the same variance as the other error displacement distances, and (2), for the cell positioning error, we do not allow the cell to extend past the end of the reflector element on which it is placed, which truncates the distribution of cell displacement errors in the upward direction.

The results of these simulations are shown in Fig. 4, in which the ensemble optical efficiency vs. tilt angle is plotted for a 1000-reflector assembly with either 15x (in panel (a)) or 7.5x (in panel (b)) concentration factor, corresponding to 1 mm or 2 mm wide cells in a 15 mm aperture, respectively. These simulations account for the finite source width of the sun, but do not consider any reflectance losses. Defining the acceptance angle as the range over which the geometric optical efficiency exceeds 95%, we see that even a 50-μm standard deviation in component position and shape can reduce the acceptance angle from 2.5 to 2.0° for the 15x geometry. The 7.5x concentrator design is considerably more forgiving, retaining a 3.7° acceptance angle even with 100 μm standard deviation in assembly error. Thus, a lower concentration factor increases both the acceptance angle, and the tolerance to manufacturing errors, though at the cost of reducing the specific power. Ultimately, the system design must account for the effects of these and other assembly errors, in addition to other factors such as deformations and pointing accuracy of the spacecraft to

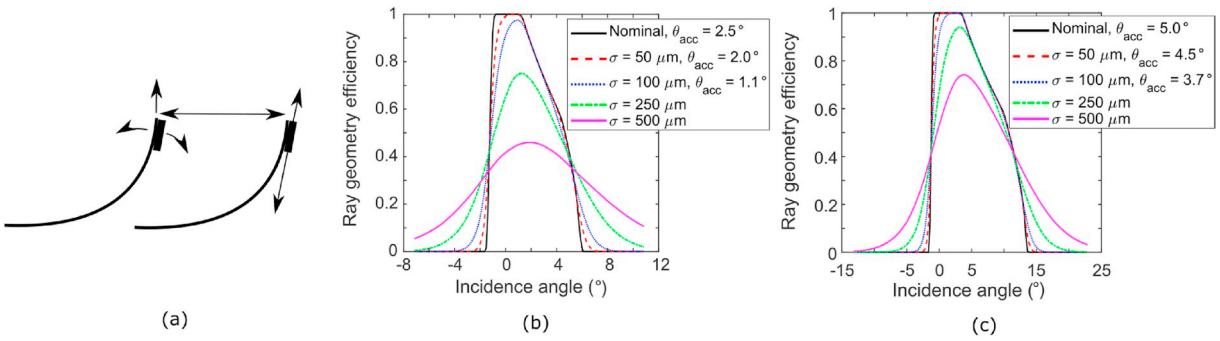


**Fig. 4.** In panel (a), schematic of shape and assembly errors varied in Monte Carlo ray tracing simulations. In panels (b–c), the ensemble geometric optical efficiency versus angle of incidence for difference precision levels for 15x and 7.5x concentration.

determine the overall optimal trade-off in specific power and acceptance angle.

### 2.2. Solar cells

#### 2.2.1. Semiconductor architecture selection

In choosing a solar cell technology for a photovoltaic array, typically three main parameters are compared: efficiency, mass, and reliability. However, when working under a concentrator system the heat load ($W/m^2$), of the cell is also critical to the success of the design. In a concentrator system, the solar power incident on the solar cell is multiplied by the concentration factor, as is the heat dissipated within the cell. Different solar cell architectures loads can exhibit wide variation in the heat flux density ($W/m^2$) that the system must conduct away from the cells and radiate to space in order to maintain the solar cells operating at a safe temperature (< 100 C). As Fig. 2 illustrated, the heat conduction requirement determines a significant component of the system mass, and therefore, the optimum multi-junction solar cell architecture in a concentrator system will combine high efficiency and low heat load.

While efficiency and waste heat load are linked for solar cells as they are for any heat engine, they do not have a simple inverse relationship. Light incident upon a solar cell will be affected in one of five ways: (1) conversion to electricity, (2) conversion to heat, (3) reemission as light, (4) reflection, or (5) transmission. The first process (electricity) determines the cell's efficiency, while the third process (reradiation) is a fundamental result of thermodynamic equilibrium established between the cell and the sun, and is naturally maximized hand-in-hand with efficiency. Conversion to heat processes include inefficiencies in the conversion of photons to electricity, unavoidable entropic losses in the cell, and parasitic absorption of light that does not contribute to electricity generation. The fifth process (transmission) does not apply to our (and most) cells since they utilize opaque back contacts. Thus, in order to minimize the heat load, we seek to maximize the cell's reflection of sunlight, to the degree we can do so without substantially reducing the amount of light converted to electricity. In doing so, we reduce the parasitic absorption and conversion inefficiency components of the heat load, because reflection and transmission losses do not change the energy of the photons involved. By placing the cell on a high-quality back reflecting mirror and adjusting the bottom band gap of the cell, the reflection losses can be adjusted to manage cell heat load. We have mapped out the opportunity space for minimizing heat load while maintaining efficiency for triple-junction solar cells by calculating the maximum theoretical efficiency achievable for solar cells with different bottom cells (lowest band gap) and the heat load associated with each design. The calculations used a simple detailed balance model (Shockley-Queisser [33]) and assumed that all the bandgap combinations would lose 20% of the calculated ideal efficiency due to non-idealities, which is a gross oversimplification but a conservative adjustment compared with performance obtained in developed materials [34]. We have also limited the maximum band of the top cell to 2.1 eV or less. The efficiency and heat load of the optimized triple-junction for each minimum band gap considered are plotted in Fig. 5 [35].

From Fig. 5, we can infer that standard Ge-based triple-junction solar cells with a minimum band gap of 0.66 eV are not optimal for concentrator photovoltaic systems. Although they can achieve a high efficiency, the heat load is ~45% higher than in cells with a similar efficiency but a bottom cell of 1.1 eV (GaInAs). This plot suggests cell design should include a band gap engineering effort focused on achieving a minimum band gap of 0.9 eV–1.1 eV. This target range for the bottom band gap suggests that an inverted metamorphic (IMM) cell is the best target for development [36]. The inverted design offers an additional benefit in that it can be placed on a high quality back

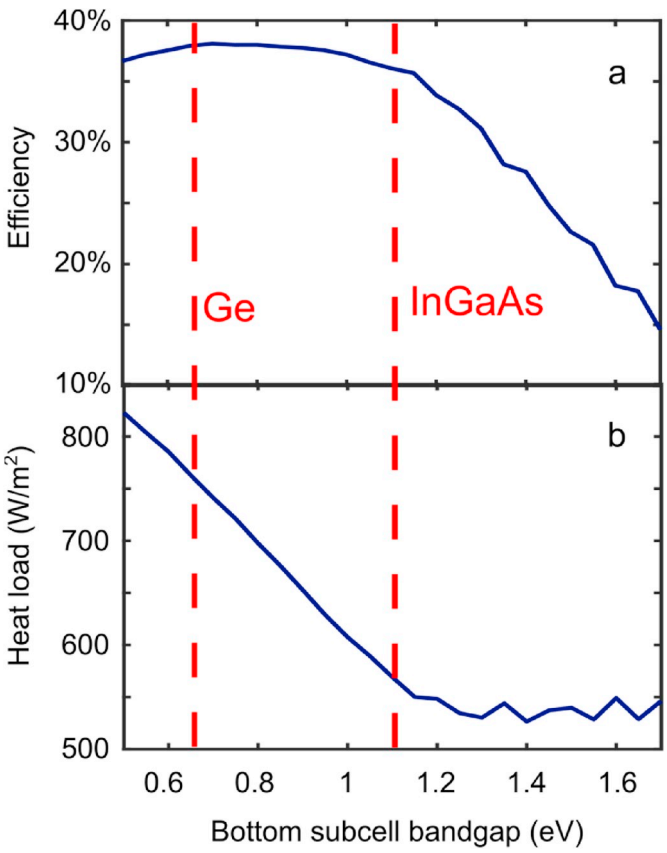


**Fig. 5.** Panel (a) shows the maximum one sun efficiency attainable for a triple junction solar cell for different bottom cell bandgap values (per detailed balance minus 20%). Panel (b) shows the heat load of these triple junction solar cells versus the bottom cell bandgap (at one sun).

reflector to reduce the cell thickness and reflect sub-bandgap photons back out of the cell before they are absorbed by free carriers or defect states in the wafer substrate. Eliminating this non-productive absorption also contributes to maintaining a low heat load compared to the Ge-based triple junction design. For these reasons, our design efforts are pursuing three and four junction IMM cells optimized to achieve efficiency of 33%–35% at 15 suns concentration and operating temperature of 80–100 C, with heat loads of 600 or fewer W/m$^2$ (at one sun). The final cell architecture configuration will be determined in detail by other constraints such as material quality, complexity of the design, thickness of the semiconductor structure, radiation hardness, and cost. Initial efforts have produced a cell with 33% efficiency at 80 C under one sun and mounted on a 27 μm Kapton film following the removal of the growth substrate [35].

#### 2.2.2. Space environment

Solar cells in space suffer radiation damage from both high and low-energy particles, necessitating the use of cover glass, typically cerium doped fused silica, to reduce the fluence of harmful particles onto the semiconductor. While this cover glass allows the cells to operate with minimal degradation for years or decades of service, it also constitutes a major component of the system mass. CPV systems reduce the mass of radiation shielding required in two ways. First, as detailed in section III, by reducing the cell area by the concentration factor. Secondly, their geometry can confer additional shielding to the solar cell, further reducing the amount of heavy cover glass required. We previously compared the front shielding needed to retain 85% of starting performance after 10 years in GEO orbit for a solar cell in a flat plate configuration and in our concentrator system [37]. In Ref. [37] we presented the results of our simulations of the environment in space with NOVICE —a 3D adjoint (reverse) Monte Carlo transport simulation program— [38]. We obtained the incident trapped electron and proton spectrums from the AE9 and AP9 models [39], respectively, and the solar protons from the JPL91 model [40]. The specifics of the concentrator mirrors were based on the earlier point design and are detailed in the above reference, and a schematic of the simulation configurations is shown in Fig. 6. Crucially, the cells in the analysis are modeled as epitaxial liftoff (ELO) cells that have been removed from their growth substrate and include a thick copper backing for support. The copper also provides backside shielding from particle radiation, in addition to the CFRP material of the mirror. Table 1 shows the ratio of the equivalent 1 MeV electron fluences for trapped electrons, trapped protons, and solar protons for the CPV design relative to the flat plate design with equivalent cover glass thickness. In all cases, the CPV design experiences lower fluences at the semiconductor surface.

The increased protection from particle radiation offered by the geometry of the CPV system comes from the structural and reflective components of the mirrors providing shielding for the cells in addition to the copper back support. This effect makes efficient use of the mass already needed for optical and thermal management functions of the design. Given this performance, the design could either further reduce the cover glass mass or the system could offer extended life, depending on the overall cost optimization.

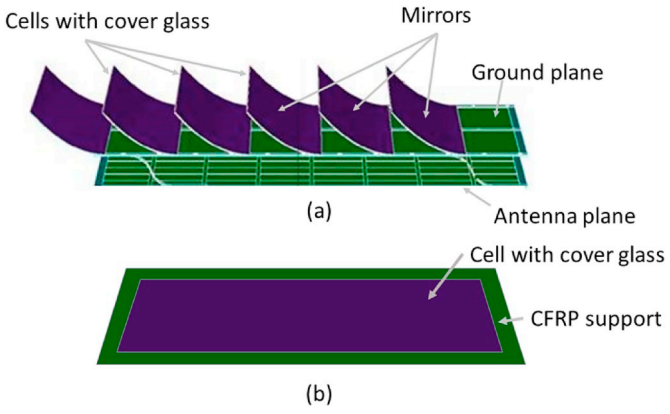


**Fig. 6.** In panel (a) a schematic view of the concentrator structure used in simulated radiation environment. In panel (b) schematic of the flat plate configuration. Both simulated structures included equal thickness cover glass over the cells.

**Table 1**
Ratio of fluences experienced by cells in CPV vs flat plate systems for different cover glass thickness and particle radiation type.

| Cover glass thickness (μm) | Trapped protons (CPV/flat) | Trapped electrons (CPV/flat) | Solar protons (CPV/flat) |
|---|---|---|---|
| 12 | 0.92 | 0.34 | 0.75 |
| 50 | 0.89 | 0.04 | 0.68 |
| 75 | 0.89 | 0.01 | 0.77 |

### 2.3. Structured coatings for enhanced thermal emission

#### 2.3.1. Mass benefits of enhanced thermal emission

While concentration is essential for achieving our target specific power, it introduces the design challenge of maintaining the photovoltaic cells below 100 C. As detailed in previous sections, the need to conduct heat away from the cell directly adds to the mass of the system, however there is a subtler additional challenge. In a flat plate design, the radiation-protective cover glass on the cells provides a high-emissivity surface that can radiate heat efficiently from the entire area of the structure. In a concentration setting, the cover glass area (and mass) are reduced and replaced with metal-coated reflective structures that do not have an inherently high emissivity. Once heat is conducted away from the cell, the design requires an effective radiation pathway to eliminate it from the structure in order to keep cell temperatures low. With effective conduction and appropriate design, the heat rejection aperture of the concentrating photovoltaic can be almost as large as the optical concentrating aperture, and cells can be maintained at temperatures only slightly higher than what they experience without concentration. Achieving this without adding substantial mass to the system requires careful attention to cell selection, as detailed above, concentration factor, and the design of high emissivity front and back surfaces.

In our concentrator design, the choice of material and thickness of the conductor structure are the only mechanisms to increase the conductance of heat from the cell. The carbon fiber composite material used to fabricate the mirrors is composed of layered plies of unidirectional graphite fibers (such as Granoc YSH pitch fibers) that can be selected from materials with a thermal conductivity of up to 250 W/m-K along the direction of the fiber, while the conductivity across the fibers is 2–3 W/m-K and dominated by the insulating properties of the resin [41]. In the layup used in our reflectors, detailed above, at minimum half of the plies are aligned with the direction of heat transfer, with at least 50% of the material offering a high conductance pathway for spreading heat away from the cells. In an ideal system, the total thickness of the CFRP would be the minimum value needed to provide sufficient thermal conductance from the cell to minimize mass. Once the cell heat is conducted throughout the area, it must be radiated away from the structure. The emissivity of the reflector surfaces, both front and back, determines the temperature profile at which the heat load can be shed. To explore this aspect of the design space we expanded the FEM simulations described above to include varying front and back surface emissivity values, as well as different CFRP thickness.

Fig. 7 panel (a) shows the cell temperature versus front and back emissivity for a cell with a 650 W/m$^2$ heat load (at one sun) in a 15 sun concentrating optic as determined by conductor thickness, front emissivity and back emissivity. The different surfaces in the plot correspond

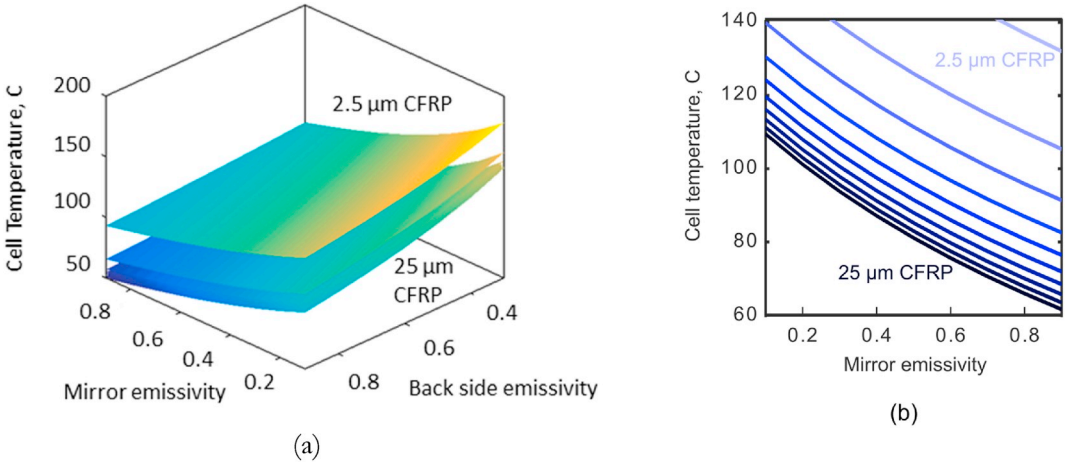


**Fig. 7.** In panel (a) cell temperature versus mirror and back surface emissivity for different thicknesses of CFPR in a symmetric four-ply layup with half of plies at zero and half at 90° relative to the concentration axis. The concentration is 15 suns and the cell has a heat load of 650 W/m$^2$ at one sun. In panel (b), a section of the plot in panel (a) for back surface emissivity value of 0.88.

to different thicknesses of CFRP conducting heat from the cell. As the slope of the surfaces shows, the cell temperature is most sensitive to changes in front mirror surface emissivity. As panel (b) shows, cell temperatures below 100 C are possible with high back surface emissivity and moderate mirror emissivity. Fortunately for the design, the CFRP material has a naturally high emissivity of 0.8–0.9 [42], meaning the design will be able to maintain cell temperatures below 100 C with low CRFP thickness provided a mirror emissivity of 0.3–0.6 can be achieved. Based on this analysis, we can identify the minimum CFRP thickness required for designs with 15 suns of concentration. If the mirror has a low emissivity, such as that of a conventional protected silver coating, the mirror will require 37 μm of CFRP for sufficient heat conduction to maintain the cell at 100 C.

#### 2.3.2. *Multilayer coatings for enhanced emissivity mirrors*

Current space applications use coatings with high thermal emissivity to enhance radiative cooling for a variety of structures and functions. These coatings are typically paints with high $TiO_2$ or $Al_2O_3$ contents, with a diffuse, high, broadband reflectivity in the visible range of the spectrum [43]. This diffuse reflectivity makes these materials unsuitable for mirror surfaces that must have high specular reflectivity in the visible and near IR.

In our previous work we have detailed the design and fabrication of high emissivity coatings based on the Salisbury screen concept [44]. These coatings, consisting of alternating layers of thin Chromium (2–4 nm) and comparatively thick CP1 polymer (~2 μm), offer emissivity values of up to 0.9 (hemispherical, averaged over 300 K black body spectrum) while adding only 3–10 g/m$^2$ to the underlying structure. These coatings also have low reflectivity in the visible and near IR, however they serve as the foundation for a new optical design. By replacing the thin Chromium layers with ITO, a transparent conductor, and using a thin silver layer for the back reflector, the multilayer coating exhibits high reflectivity in the visible-near IR target range while retaining substantial 300 K emissivity. Fig. 8 shows a schematic of this optical structure (panel a, not to scale), the reflectivity in the visible (panel b, simulated), and the absorptivity in the IR (panel c, simulated). Averaged over the hemisphere, this coating achieves a reflectivity of 89.6% in the visible (weighted by the AM0 spectrum) and an emissivity of 0.55 (weighted by the 300 K black body spectrum) while adding only 4.07 g/m$^2$ to the system. When placed onto the CFRP parabolas as the reflective surface, the combined optical efficiency of the mirror will be 87.81%. With this front surface emissivity, the CFRP thickness required to maintain the cell at 100 C decreases from 37 μm to 10 μm, representing a substantial mass reduction.

## 3. Conclusion

The sections above detail the development and optimization of multiple key technological elements that are all crucial for the success of the design concept. Combining the performance of the individual design elements detailed above allows us to estimate the total system performance in terms of efficiency, power produced per square meter, areal mass density and specific power and explore how these design elements combine to enable large increases in specific power. Table 2 outlines these results, showing these performance parameters for space PV designs starting with commercially available cover glass-interconnected cells (CIC) from the SolAero IMM-α data sheet and representing the current status of flat plate technology [45]. Next the table shows a substantial improvement for a one-sun PV design using high efficiency multijunction cells: a 10 μm ELO cell with 20 μm of copper on the back and 75 μm of cover glass, plus adhesive mounted on a 5 μm Kapton HN membrane with carbon fiber support frame at the perimeter for structural support. These one-sun designs operate at 32% and 33% efficiency respectively, and the reduction in mass from the CIC increases the specific power from 0.5 to 1 kW/kg.

Next the table places that mass-optimized ELO cell, including copper backing and cover glass, into a 7.5 sun concentrator with a 15 mm aperture and mirror CFRP thickness of 37 μm, sufficient to conduct heat away from the 2 mm wide cell and have it radiate from a high-reflectivity (low emissivity) mirror with a conventional protected silver coating. The mass of this design configuration still includes the Kapton HN membrane with CFRP frame and now also includes the contact traces, support and adhesive required to mount the cells on the mirror. At 7.5 suns, this design somewhat compromises its specific power, at 3 kW/kg in order to retain a larger acceptance angle of around ± 2.5°. If the accuracy of manufacturing and spacecraft pointing can match the ambition of the concentrator module, higher specific power still can be attained by increasing the concentration to 15 suns with an acceptance angle of ± 1.25°. The higher concentration design can be considered in two configurations. First, with the ELO solar cell and radiation protection detailed above at a width of 1 mm and placed in the same 15 mm aperture with 37 μm CFRP mirrors. With a high reflectivity ("low emissivity") silver mirror this configuration will have a specific power of 3.7 kW/kg, again including the Kapton HN membrane and contact traces. This presents a more than seven-fold increase over the CIC specific power. In the second case, the ELO cell, membrane support and contact traces remain the same, however the mirrors will have the reflective structured coating on the mirror surface ("low reflectivity") and the mirror CFRP thickness can be reduced to 10

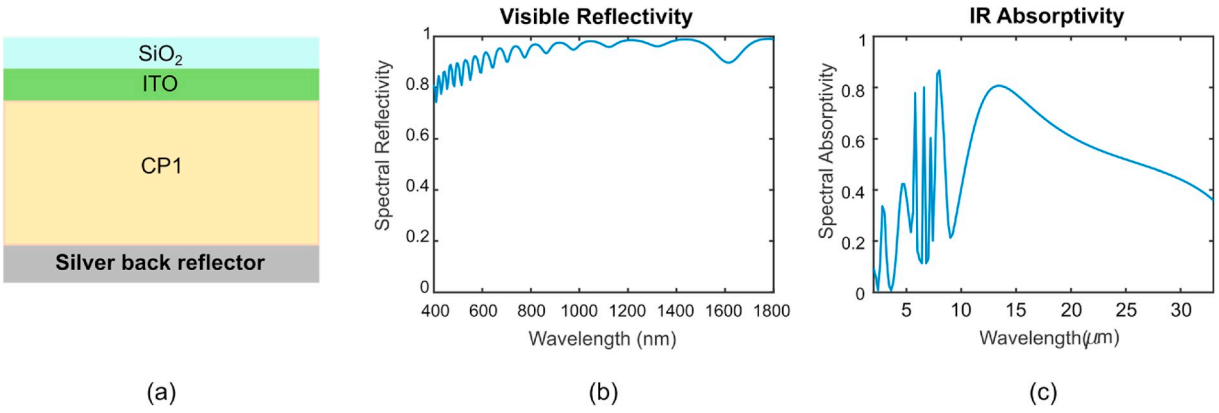


**Fig. 8.** Schematic (not to scale) of layer structure of visibly reflective Salisbury screen design with 60 nm of SiO2, 10 nm of ITO and 2.3 μm of CP1 polyimide on a silver back reflector (a), simulated spectral reflectivity of the design in the visible and near-IR (b), and simulated absorptivity of the structure over the mid-IR region relevant to the 300 K black body spectrum.

**Table 2**
Area mass density, area power density, efficiency and specific power of various design scenarios for the concentrating space PV concept as well as a flat plate, non-concentrating baseline.

| Configuration | g/m$^2$ | W/m$^2$ | Efficiency | kW/kg |
|---|---|---|---|---|
| CIC | 833 | 437 | 32% | 0.52 |
| Flat plate | 476 | 451 | 33% | 0.95 |
| 7.5X low emissivity | 145 | 431 | 32% | 3.0 |
| 15X low emissivity | 115 | 431 | 32% | 3.7 |
| 15X low reflectivity | 96 | 396 | 29% | 4.1 |

μm with the improved radiation of heat from the cell. By reducing the CFRP material, the mass per area of this 15 sun configuration is only 96 g/m$^2$, however the lower reflectivity of the mirror decreases the optical efficiency of the design and reduces the power per area compared to the low emissivity case. The specific power of the low reflectivity case is projected to be 4.1 kW/kg, almost eight times the current state of the art for the CIC product. This table omits any deployment mechanisms or additional structure required for integration in the final application.

If broader system considerations require a higher power output from the PV subsystem either to improve efficiency in the transmission electronics or to reduce the number of space craft needed to achieve a given power rating, the low emissivity PV configuration may be preferable for its higher power per area. For example, if the packaging of the final system results in a launch payload constrained by volume rather than by mass, the higher power per area might allow a smaller number of launches and lower overall cost even with larger mass. Conversely if the mass of the PV subsystem is most critical for system viability, the low reflectivity configuration may be preferred for its higher specific power. Ultimately the final design configuration will be determined by larger system performance trade-offs as well as by fabrication cost, which we have not yet incorporated into these calculations.

It is important to note that, although the component technologies utilized in these designs have been extensively developed and tested in space applications (e.g., CFRP composites, III-V solar cells, …), the concentrators presented here will require ambitious improvements in ultrathin CFRP mirror technology in order to achieve the required optical precision with such thin materials. A simple challenge is that such thin plies of pitch fiber prepreg material are not yet commercially available. If such materials cannot be developed or cannot be reliably cast in the required parabolic form, then it would become necessary to use thicker materials than called for here, which would reduce the specific power of the designs. Current prototyping efforts, shown in Fig. 9, have reduced mirror thickness to ~140–180 μm. Should this thickness range prove to be a lower limit, the additional CFRP mass beyond that included in Table 2 would reduce the specific power of the designs by roughly 50%. With that caveat, the design approach and analysis detailed here point to the possibility of substantial improvements above currently available technology. Both the low emissivity and low reflectivity configurations can achieve specific power levels that are more than 7 times higher than the current state-of-the-art for space photovoltaic systems, at 3.7 kW/kg and 4.1 kW/kg respectively. Efforts to prototype this design at small scale and integrate the PV system with power transmission subsystem are ongoing, with efforts to be detailed further in subsequent publications.

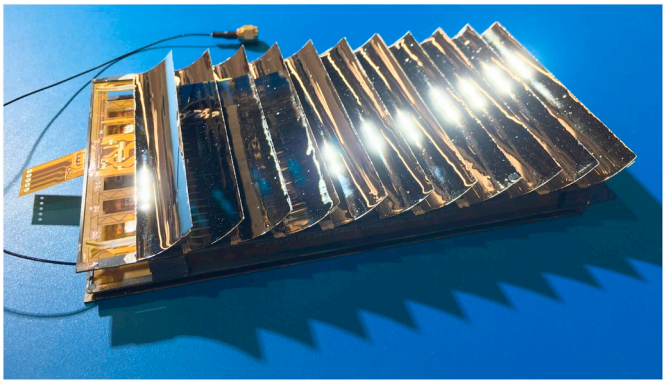

**Fig. 9.** Photograph of integrated tile prototype including concentrating photovoltaics, microwave drive electronics and antenna plane.

## Acknowledgment

This work has been supported by funding from the Northrop Grumman Corporation and the Caltech Space Solar Power Project.

## References

[1] I. Asimov, Reason, Astounding Sci. Fict, (1941), pp. 33–45.
[2] J.C. Mankins, A Fresh Look at Space Solar Power : New Architectures , Concepts and Technologies, (1997), pp. 6–17, https://doi.org/10.1016/S0094-5765(98)00075-7 Aiaa.
[3] D. On E. and P.S. Committee for the Assessment of NASA's Space Solar Power Investment Strategy, Aeronautics and Space Engineering Board, Laying the Foundation for Space Solar Power: an Assessment of NASA's Space ... - National Research Council, Division on Engineering and Physical Sciences, Aeronautics and Space Engineering Board, Committee for the Assessment of NASA's Space Solar Power Investment Strategy - Google Books, (2001) https://books.google.com/books?hl=en&lr=&id=KZucAgAAQBAJ&oi=fnd&pg=PR1&dq=Laying+the+foundation+for+space+solar+power:+An+assessment+of+NASA , Accessed date: 23 August 2018s+space+solar+power+investment+strategy&

ots=-AEhsXad06&sig=uZJyQggp8gbkQoEIbuPfjM42K-M#v=onepage&q=Laying%25 '.
[4] J.W.S.R.H. Dietz, G.D. Amdt, J.S.K.L. Leopold, Satellite power system: concept development and evaluation program, NASA ref. Publ. 1076 vol. 111 - power transm, Recept. Tech. Summ. Assess. (1981), https://doi.org/10.2172/6357340.
[5] R. Kasper, Electric power from orbit: a critique of a satellite power system, Unknown 82 (1981), http://adsabs.harvard.edu/abs/1981STIN...8227858K , Accessed date: 23 August 2018.
[6] I. Cash, CASSIOPeiA solar power satellite, 2017 IEEE Int. Conf. Wirel. Sp. Extrem. Environ. WiSEE 2017 vol. 2, (2017), pp. 144–149, https://doi.org/10.1109/WiSEE.2017.8124908.
[7] J. Mankins, N. Kaya, M. Vasile, SPS-ALPHA: the first practical solar power satellite via arbitrarily large phased array (A 2011-2012 NIAC Project), 10th Int. Energy Convers. Eng. Conf. American Institute of Aeronautics and Astronautics, Reston, Virigina, 2012, , https://doi.org/10.2514/6.2012-3978.
[8] N. Goswami, China in space ambitions and possible conflict, Strateg. Stud. Q. 12 (2018) 74–97, https://doi.org/10.5837/bjc.2014.024.
[9] M. Mori, H. Kagawa, Y. Saito, Summary of studies on space solar power systems of Japan Aerospace Exploration Agency (JAXA), Acta Astronaut. 59 (2006) 132–138, https://doi.org/10.1016/J.ACTAASTRO.2006.02.033.
[10] S. Sasaki, K. Tanaka, K. Maki, Microwave power transmission technologies for solar power satellites, Proc. IEEE 101 (2013) 1438–1447, https://doi.org/10.1109/JPROC.2013.2246851.
[11] B.P. Jaffe, J. McSpadden, Energy conversion and transmission modules for space solar power an exhaustive and historical background of SSP developments in connection with, Proc. IEEE 101 (2013), https://doi.org/10.1109/JPROC.2013.2252591.
[12] M.D. Kelzenberg, P. Espinct-Gonzalez, N. Vaidya, T.A. Roy, E.C. Warmann, A. Naqavi, S.P. Loke, J.-S. Huang, T.G. Vinogradova, A.J. Messer, C. Leclerc, E.E. Gdoutos, F. Royer, A. Hajimiri, S. Pellegrino, H.A. Atwater, Design and prototyping efforts for the space solar power initiative, 2017 IEEE 44th Photovolt. Spec. Conf. IEEE, 2017, pp. 558–561, , https://doi.org/10.1109/PVSC.2017.8366621.
[13] E. Gdoutos, C. Leclerc, F. Royer, M.D. Kelzenberg, E.C. Warmann, P. Espinet-Gonzalez, N. Vaidya, F. Bohn, B. Abiri, M.R. Hashemi, M. Gal-Katziri, A. Fikes, H. Atwater, A. Hajimiri, S. Pellegrino, A lightweight tile structure integrating photovoltaic conversion and RF power transfer for space solar power applications, 2018 AIAA Spacecr. Struct. Conf. American Institute of Aeronautics and Astronautics, Reston, Virginia, 2018, , https://doi.org/10.2514/6.2018-2202.
[14] B. Carpenter, J. Banik, P. Hausgen, Roll-out solar arrays (ROSA): next generation flexible solar array technology, AIAA Sp. Astronaut. Forum Expo. American Institute of Aeronautics and Astronautics, Reston, Virginia, 2017, , https://doi.org/10.2514/6.2017-5307.
[15] T.G. Stern, K. Steele, Flexible solar array with structural photovoltaic assembly, 2015 IEEE 42nd Photovolt. Spec. Conf. PVSC 2015, 2015, https://doi.org/10.1109/PVSC.2015.7355946.
[16] D. Campbell, R. Barrett, M.S. Lake, L. Adams, E. Abramson, M.R. Scherbarthn, J.S. Welsh, G. Freebury, N. Beidleman, J. Abbot, Development of a novel, passively deployed roll-out solar array, 2006 IEEE Aerosp. Conf. vol. 298, (2006), pp. 1–9, https://doi.org/10.2514/6.2006-4011.
[17] M. Tafazoli, A study of on-orbit spacecraft failures, Acta Astronaut. 64 (2009) 195–205, https://doi.org/10.1016/J.ACTAASTRO.2008.07.019.
[18] M.J. O'Neill, A.J. McDanal, M.F. Piszczor, M.I. Eskenazi, P.A. Jones, C. Carrington, D.L. Edwards, H.W. Brandhorst, The stretched lens ultralight concentrator array, Conf. Rec. Twenty-Eighth IEEE Photovolt. Spec. Conf. - 2000 (Cat. No.00CH37036), IEEE, 2000, pp. 1135–1138, , https://doi.org/10.1109/PVSC.2000.916087.
[19] M.O. Neill, A.J.J. McDanal, M. Piszczor, M. Myers, P. Sharps, C. Mcpheeters, J. Steinfeldt, M.O. Neill, N. Glenn, M. Oneill, A.J.J. McDanal, M. Piszczor, M. Myers, P. Sharps, C. Mcpheeters, J. Steinfedt, Line-focus and point-focus space photovoltaic concentrators using robust fresnel lenses , 4-junction cells , & graphene radiators, IEEE 44th Photovolt. Spec. Conf. IEEE, 2017, pp. 525–530, , https://doi.org/10.1109/PVSC.2017.8366596.
[20] M. O'Neill, A.J. McDanal, G. Landis, R. Pricone, C. Kumar, M. Puglia, Space PV Concentrators for outer planet and near-sun missions, using ultra-light fresnel lenses made with vanishing tools, IEEE 46th Photovolt. Spec. Conf. IEEE, Chicago, 2019.
[21] T.G. Stern, Interim results of the SLATS concentrator experiment on LIPS-III, Proc. 20th IEEE Photovoltaics Spec. Converence. (1988), https://doi.org/10.1109/PVSC.1988.105822.
[22] T.G. Stern, Initial performance tests of SLATS photovoltaic concentrator modules, IEEE Photovolt. Spec. Conf. 19th, New Orleans, LA, May 4-8, 1987, 1987, pp. 439–441 http://adsabs.harvard.edu/abs/1987pvsp.conf..439S , Accessed date: 22 August 2018.
[23] J.H. Ermer, R.K. Jones, P. Hebert, P. Pien, R.R. King, D. Bhusari, R. Brandt, O. Al-Taher, C. Fetzer, G.S. Kinsey, N. Karam, Status of C3MJ+ and C4MJ production concentrator solar cells at spectrolab, IEEE J. Photovolt. 2 (2012) 209–213, https://doi.org/10.1109/JPHOTOV.2011.2180893.
[24] J. Steeves, S. Pellegrino, Ultra-thin highly deformable composite mirrors, 54th AIAA/ASME/ASCE/AHS/ASC Struct. Struct. Dyn. Mater. Conf. American Institute of Aeronautics and Astronautics, Reston, Virginia, 2013, , https://doi.org/10.2514/6.2013-1523.
[25] A.A. Abusafieh, D.R. Federico, S.J. Connell, E.J. Cohen, P.B. Willis, Dimensional stability of CFRP composites for space-based reflectors, in: A.E. Hatheway (Ed.), Proc. SPIE, Optomechanical Design and Engineering 2001, San Diego, CA, 2001, pp. 9–16, , https://doi.org/10.1117/12.447300.
[26] H. Lengsfeld, F. Wolff-Fabris, J. Krämer, J. Lacalle, V. Altstädt, H. Lengsfeld, M. Turner, Prepreg Technology, in: Compos. Technol. Hanser, 2016, pp. 27–45, https://doi.org/10.3139/9781569906002.003.
[27] M.A. Bessa, S. Pellegrino, Design of ultra-thin composite deployable shell structures through machine learning, Proc. IASS Annu. Symp. (2017) 1–8 http://www.its.caltech.edu/~sslab/PUBLICATIONS/MABessa_IASS17_MachineLearning_article_final.pdf.
[28] N. Vaidya, M.D. Kelzenberg, P. Espinet-Gonzalez, T.G. Vinogradova, J.-S. Huang, C. Leclerc, A. Naqavi, E.C. Warman, S. Pellegrino, H.A. Atwater, Lightweight carbon fiber mirrors for solar concentrator applications, 2017 IEEE 44th Photovolt. Spec. Conf. IEEE, 2017, pp. 572–577, , https://doi.org/10.1109/PVSC.2017.8366046.
[29] N. Vaidya, O. Solgaard, 3D printed optics with nanometer scale surface roughness, Microsyst. Nanoeng. 4 (2018) 18, https://doi.org/10.1038/s41378-018-0015-4.
[30] Outgassing Data for Selecting Spacecraft Materials System, (n.d.). https://outgassing.nasa.gov/(accessed November 27, 2018).
[31] C. Decker, The use of UV irradiation in polymerization, Polym. Int. 45 (1998) 133–141, https://doi.org/10.1002/(SICI)1097-0126(199802)45:2<133::AID-PI969>3.0.CO;2-F.
[32] State of the Art of Small Spacecraft Technology, (n.d.). https://sst-soa.arc.nasa.gov/ (accessed November 21, 2018).
[33] W. Shockley, H.J. Queisser, Detailed balance limit of efficiency of p-n junction solar cells, J. Appl. Phys. 32 (1961) 510.
[34] R.M. France, J.F. Geisz, M.a. Steiner, D.J. Friedman, J. Scott Ward, J.M. Olson, W. Olavarria, M. Young, A. Duda, Pushing inverted metamorphic multijunction solar cells toward higher efficiency at realistic operating conditions, IEEE J. Photovolt. 3 (2013) 893–898, https://doi.org/10.1109/JPHOTOV.2013.2239358.
[35] P. Espinet-gonzalez, R.M. France, M.D. Kelzenberg, J.F. Geisz, E.C. Warmann, N. Vaidya, S.P. Loke, D.J. Friedman, H.A. Atwater, Inverted metamorphic triple-junction solar cells on polyimide substrate for concentrator photovoltaic systems in space, 2018 IEEE 7th World Conf. Photovolt. Energy Convers. (A Jt. Conf. 45th IEEE PVSC, 28th PVSEC 34th EU PVSEC), 2018.
[36] J.F. Geisz, D.J. Friedman, J.S. Ward, A. Duda, W.J. Olavarria, T.E. Moriarty, J.T. Kiehl, M.J. Romero, A.G. Norman, K.M. Jones, 40.8% efficient inverted triple-junction solar cell with two independently metamorphic junctions, Appl. Phys. Lett. 93 (2008) 12350510.1063/1.2988497.
[37] P. Espinet-Gonzalez, T.G. Vinogradova, M.D. Kelzenberg, A. Messer, E.C. Warmann, C. Peterson, N. Vaidya, A. Naqavi, J. Huang, S. Loke, D. Walder, C. Mann, S. Pellegrino, H.A. Atwater, Impact of space radiation environment on concentrator photovoltaic systems, IEEE 44th Photovolt. Spec. Conf. 2017.
[38] I. Jun, S. Kang, R. Evans, M. Cherng, Radiation Transport Tools for Space Applications: A Review Space Applications: A Review, (2008) https://trs.jpl.nasa.gov/bitstream/handle/2014/41523/08-4571.pdf?sequence=1 , Accessed date: 29 January 2019.
[39] G.P. Ginet, T.P. O'Brien, S.L. Huston, W.R. Johnston, T.B. Guild, R. Friedel, C.D. Lindstrom, C.J. Roth, P. Whelan, R.A. Quinn, D. Madden, S. Morley, Y.-J. Su, AE9, AP9 and SPM: new models for specifying the trapped energetic particle and space plasma environment, Van Allen Probes Mission, Springer US, Boston, MA, 2013, pp. 579–615, , https://doi.org/10.1007/978-1-4899-7433-4_18.
[40] J. Feynman, G. Spitale, J. Wang, S. Gabriel, Interplanetary proton fluence model: JPL 1991, J. Geophys. Res. Sp. Phys. 98 (1993) 13281–13294, https://doi.org/10.1029/92JA02670.
[41] C.A. Silva, E, M Schuller Marotta, L. Peel, M. O'Neill, In-plane thermal conductivity in thin carbon fiber composites, J. Thermophys. Heat Tran. 21 (2007) 460–467, https://doi.org/10.2514/1.27859.
[42] G. Neuer, Spectral and total emissivity measurements of highly emitting materials, Int. J. Thermophys. 16 (1995) 257–265, https://doi.org/10.1007/BF01438976.
[43] D.G. Gilmore, Spacecraft Thermal Control Handbook, Aerospace Press, 2002.
[44] A. Naqavi, S.P. Loke, M.D. Kelzenberg, D.M. Callahan, T. Tiwald, E.C. Warmann, P. Espinet-González, N. Vaidya, T.A. Roy, J. Huang, T.G. Vinogradova, H.A. Atwater, Extremely broadband ultralight thermally-emissive optical coatings, Optic Express 26 (2018) 18545, https://doi.org/10.1364/OE.26.018545.
[45] IMM-alpha Space Solar Cell Datasheet, (n.d.). https://solaerotech.com/wp-content/uploads/2018/04/IMM-alpha-Preliminary-Datasheet-April-2018-v.1.pdf (accessed September 13, 2019).